AGU PUBLICATIONS

Geophysical Research Letters

RESEARCH LETTER
10.1002/2015GL065544

Key Points:
- Widespread wind-scour zones impact surface mass balance over Recovery Ice Stream catchment
- Radiostratigraphy shows gradual ablation of ~200 years of accumulation in East Antarctica
- The mass loss over the wind-scour zones is mostly by sublimation with little redeposition

Supporting Information:
- Texts S1–S6, Figures S1–S8, and Table S1

Correspondence to:
I. Das,
indrani@ldeo.columbia.edu

Citation:
Das, I., T. A. Scambos, L. S. Koenig, M. R. van den Broeke, and J. T. M. Lenaerts (2015), Extreme wind-ice interaction over Recovery Ice Stream, East Antarctica, *Geophys. Res. Lett.*, *42*, 8064–8071, doi:10.1002/2015GL065544.

Received 27 JUL 2015
Accepted 2 SEP 2015
Accepted article online 11 SEP 2015
Published online 12 OCT 2015

Extreme wind-ice interaction over Recovery Ice Stream, East Antarctica

Indrani Das[1], Ted A. Scambos[2], Lora S. Koenig[2], Michiel R. van den Broeke[3], and Jan T. M. Lenaerts[3]

[1]Lamont Doherty Earth Observatory, Columbia University, Palisades, New York, USA, [2]National Snow and Ice Data Center, University of Colorado Boulder, Boulder, Colorado, USA, [3]Institute for Marine and Atmospheric Research Utrecht, Utrecht University, Utrecht, Netherlands

Abstract Surface snow accumulation over East Antarctica is an important climate indicator but a difficult parameter to constrain. Surface mass ablation dominates over persistent wind-scour zones as near-surface katabatic winds accelerate over locally steeper ice surface topography, and sublimate and redistribute snow. Here we quantify ablation rates and downwind redeposition of snow over wind-scour zones in the upper Recovery Ice Stream catchment. Airborne radio echo-soundings show a gradual ablation of ~16–18 m of firn, corresponding to ~200 years of accumulation, over these zones and ablation rates of ~54 kg m^{-2} a^{-1} (54 mm water equivalent a^{-1}). We conclude that mass loss is dominated by sublimation and mass is transported downwind as water vapor, because snow redeposition downslope of the wind-scour zones constitutes only a small fraction (<10%) of the cumulative mass loss.

1. Introduction

Wind-induced ablation of surface snow is a persistent phenomenon in East Antarctica. The ice sheet's surface mass balance (SMB) is decreased when katabatic winds sublimate the blowing and drifting snow [*Lenaerts et al.*, 2012a] or when wind-blown snow is transported to the ocean in the coastal regions [*Goodwin*, 1990; *Palm et al.*, 2011; *Scarchilli et al.*, 2010]. Reduced snow accumulation by blowing, drifting, and sublimation has been extensively studied by ground-based and satellite observations, and modeling [*Arcone et al.*, 2012; *Das et al.*, 2013; *Fahnestock et al.*, 2000; *Frezzotti et al.*, 2007; *Lenaerts et al.*, 2012b; *Palm et al.*, 2011; *Scambos et al.*, 2012]. Yet the process has proved to be complex and difficult to constrain by any single method. Extensive areas of wind-scour zones (regions of zero to negative SMB) are predicted in East Antarctica [*Das et al.*, 2013] and observed as surface glaze using satellite data [*Scambos et al.*, 2012]. Wind-scour zones cover ~7% of the surface area of Antarctica and are tied to small-scale topography not fully resolved in continental digital elevation models. Mass budget methods for mass balance estimates rely heavily on SMB rates from regional climate models (RCMs). In this paper, we demonstrate that overestimating the SMB can contribute to the overly positive mass balance rates using mass budget method compared to satellite radar altimetry over major East Antarctic glaciers including the Recovery Ice Stream [*Shepherd et al.*, 2012].

Sublimation of surface snow over wind-scour zones is a complicated and self-limiting process that depends on many factors, including exchange of heat, momentum and moisture with the surface, turbulent mixing due to surface roughness, saturation of the lower atmosphere, and the intensity of the katabatic winds [*Barral et al.*, 2014; *Bintanja*, 2000; *Frezzotti et al.*, 2013; *Van den Broeke*, 1997]. So far, direct measurements of sublimation rates over East Antarctica come from sparse ground traverses; e.g., *Frezzotti et al.* [2007] and very few data points actually exist over a wind-scoured surface. Our objective is to quantify the rates of accumulation and ablation over wind-scoured zones using shallow ice radar, ice cores, ice surface velocity, high-resolution satellite data, and RCM output over the upper catchment of Recovery Ice Stream, East Antarctica.

2. Study Area and Data Sets

The Recovery Ice Stream is one of the several regions of East Antarctica where mass balance rates using models and satellite radar altimetry differ [*Shepherd et al.*, 2012]. Persistent wind-scour zones have been predicted in this region using thresholds of mean slope in the wind direction (MSWD $\geq$ 0.002), accumulation (A), and wind speed (W) (A/W < 9.12) [*Das et al.*, 2013] (Figures 1a–1c). MSWD is a dot product of the mean annual wind vector with the gradient of surface slope [*Das et al.*, 2013; *Frezzotti et al.*, 2002; *Scambos et al.*, 2012].

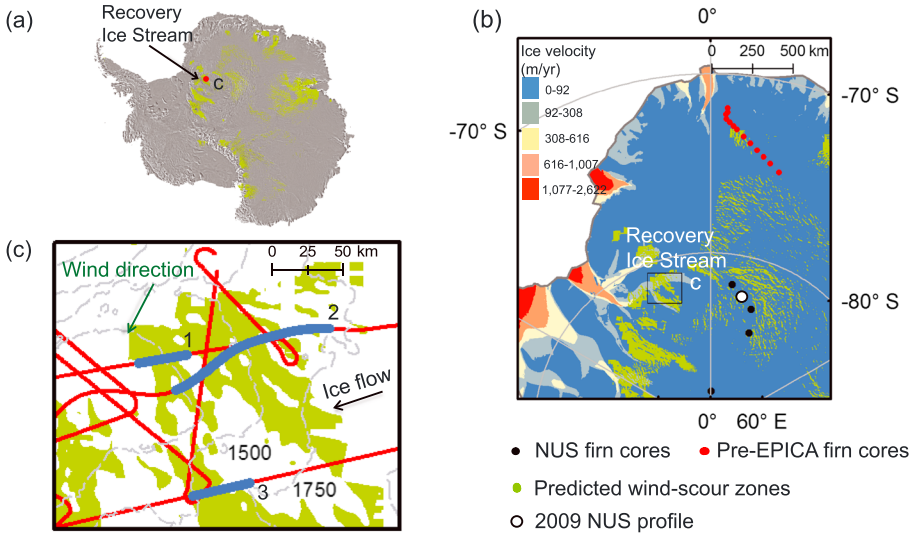

Figure 1. Study area over Recovery Ice Stream, Antarctica. (a) Study area (red), continent-wide predicted wind-scour zones (green) [*Das et al.*, 2013]. (b) Ice surface velocity [*Rignot et al.*, 2011], firn core locations, and the study area (box) in Figure 1c. (c) Profiles 1–3 (blue) over predicted wind-scour zones (green), surface elevation contours at 250 m intervals (grey) [*Bamber et al.*, 2009], and IceBridge flight lines (red).

Here we use IceBridge (CReSIS) airborne snow radar (2–6.5 GHz) [*Medley et al.*, 2014] and laser altimetry data from 2011. For processing depth and SMB from radar-echo sounding we use dielectric permittivity and density profiles from 17 shallow firn cores (10 and 30 m deep; Figure 1b) collected during the 2008/2009 U.S.-Norway (NUS) traverse [*Anschütz et al.*, 2011] and the 1996/1997 European Project for Ice Coring in Antarctica presite survey in Dronning Maud Land [*van den Broeke et al.*, 1999]. We chose our study area based on the predicted wind-scour zones, availability of ice cores and airborne radar data. We use profile sections (Profiles 1, 2, and 3; Figures 1c, 3, and S1 in the supporting information) over the scour zones for deriving SMB rates. In order to provide time scales to Profiles 1–3, we use an ice core-dated NUS radar profile from 2009 (hereafter "2009 NUS profile"; Figure 2a) [*Anschütz et al.*, 2011] collected using a ground-penetrating radar (1.75 GHz, bandwidth 2.5 GHz) and located ~490 km southeast of the study area (Figure 1b).

We use the Regional Atmospheric Climate MOdel version 2.3 (RACMO2.3) [*van Wessem et al.*, 2014] to provide wind speed and direction and accumulation rates for comparison with the radar-derived SMB. Snow grain size is derived using Moderate Resolution Imaging Spectroradiometer (MODIS) [*Scambos et al.*, 2012]. Ice surface velocities are provided by interferometric synthetic aperture radar (InSAR) techniques [*Rignot et al.*, 2011].

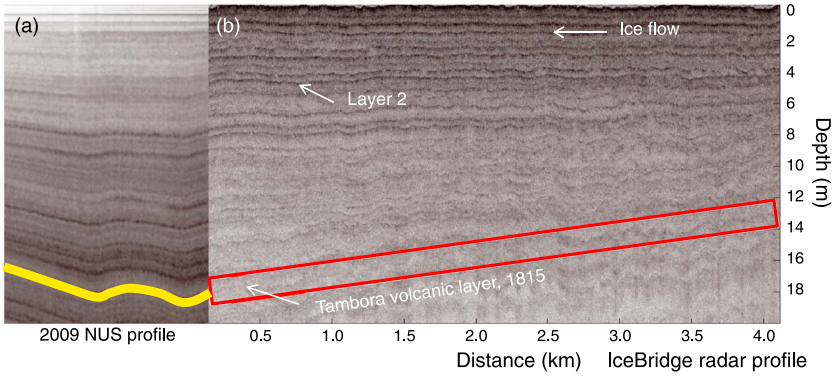

Figure 2. Identifying the Tambora volcanic layer in IceBridge snow radar. (a) The 2009 NUS profile with the Tambora layer (yellow) [*Anschütz et al.*, 2011]. (b) IceBridge snow radar-Tambora layer and Layer 2 (near the Agung volcanic peak). The red rectangle is the 2 m window used as uncertainty in identifying the Tambora layer in IceBridge profiles.

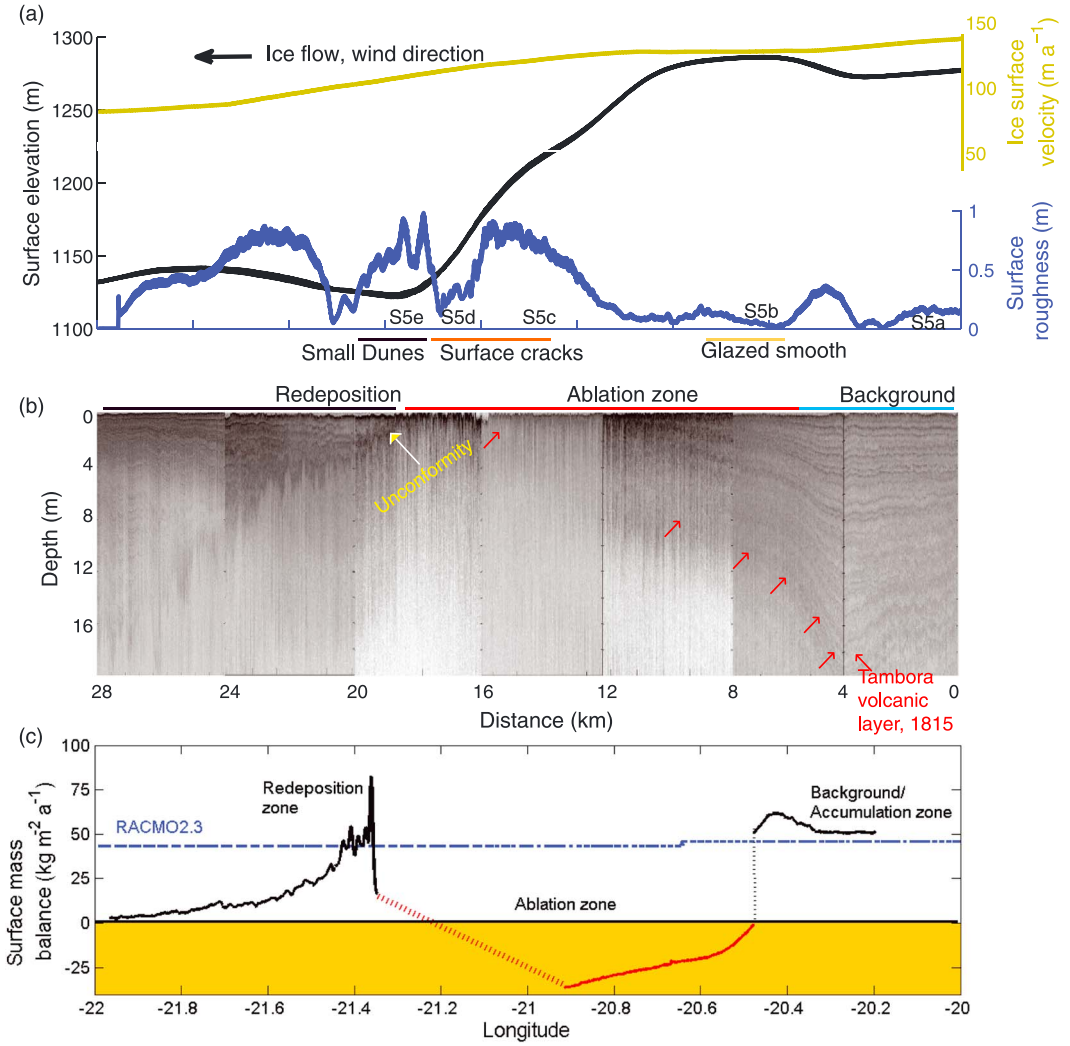

Figure 3. Variation of SMB along Profile 1. (a) Surface elevation (black), surface roughness (blue), and ice surface velocity (yellow). The surface roughness (glaze, crack, and dunes) corresponds to the WorldView imageries in Figure S5. (b) Snow radar showing truncation of internal layers starting around 8 km, location (arrows) of the Tambora layer (red), the unconformity (yellow). (c) SMB rates over the accumulation, ablation, and redeposition zones compared with RACMO2.3 SMB rates (blue). The red dashed line indicates extrapolated SMB after the Tambora layer is presumably ablated.

3. Deriving Accumulation Rates From Snow Radar

3.1. Depth-Density Profiles and Accumulation Rates

We focus on a concentration of larger wind-scour zones delineated in the snow radar profiles (Figures 1b, 3 and 4, and S1). Within these profiles, we identify normal accumulation regions where the internal layers parallel the ice surface, wind-scour zones with truncated internal layers indicating ablation, and downslope redeposition zones where unconformities bound the onlapping strata (e.g., Figure 3b). The two-way travel times of the radar profiles are converted to depth using NUS08 ice cores and standard techniques [e.g., *Sinisalo et al.*, 2013] (Text S2 in the supporting information).

In the 2011 IceBridge radar data sets we use the volcanic signal associated with the Tambora eruption from 1815 as an absolute time marker to calculate SMB in the normal accumulation regions and the wind-scour zones (section 3.2). We use the unconformity as a time marker to calculate SMB rates in the redeposition zones assuming that its continuity results from a buried, wind-scoured, and hardened surface (Figure 3b).

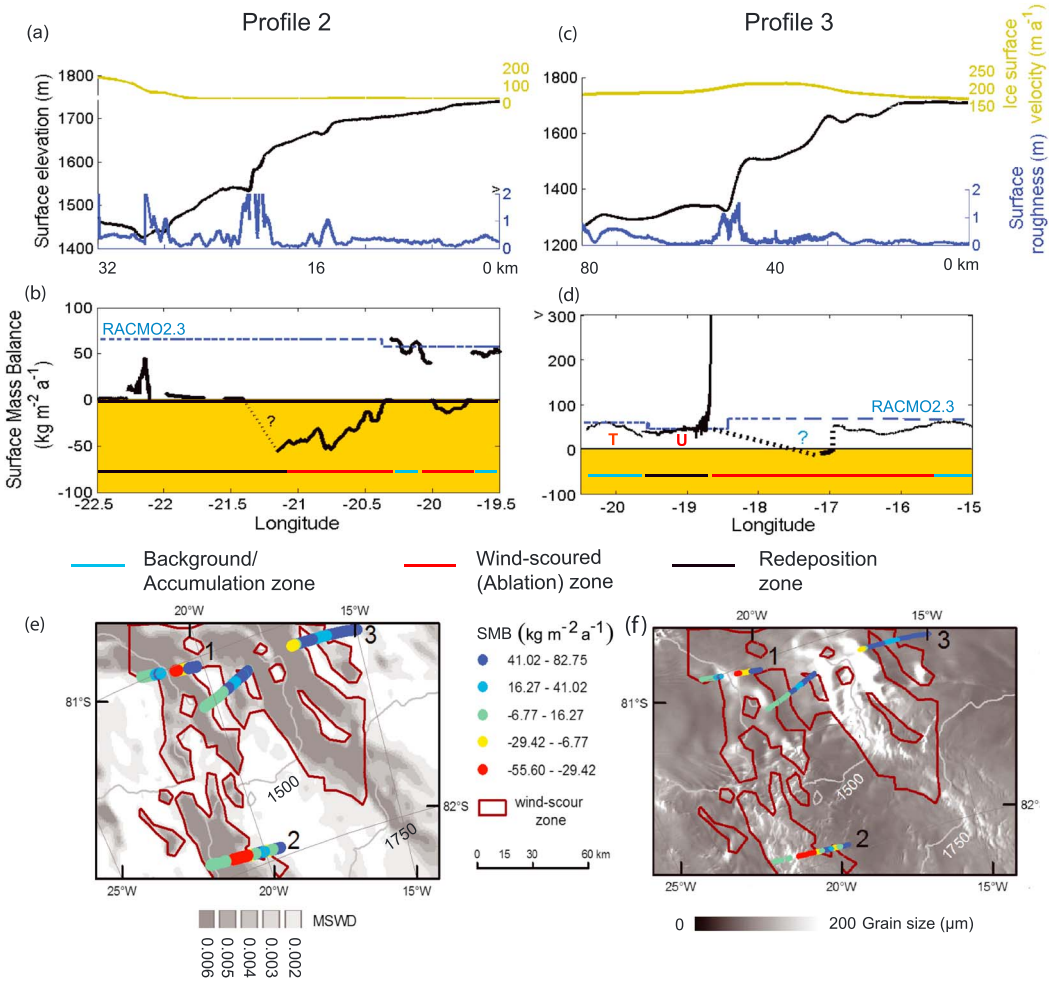

Figure 4. (a–d) Surface elevation, roughness, ice velocity, and SMB rates along Profiles 2 and 3; Variation of SMB rates over the wind-scour zones and correlation with (e) mean slope in the wind direction; (f) grain size from MODIS.

For SMB estimates using the Tambora layer we use mean density derived from the ensemble of 17 firn cores distributed along the Recovery Highlands to the coast (Figures 1b and S2, black profile). We assume that this mean density profile represents our study area well and captures any density variation in the Recovery region from the interior to the coast.

We expect that the redeposition zones, where the unconformities originate, should consist of a mixture of fresh snow, eroded firn from the wind-scour zones and diamond dust. To account for this mixture, we use a density of 350 kg m^{-3}, an average derived using surface densities from the mean density profile and the wind-hardened regions (black and red profiles, respectively; Figure S2 and Text S2.2). This density is used for all SMB calculations using the unconformity.

SMB rates are calculated using the standard equation for converting depth from a radar profile to accumulation rates, such that

$$\mathrm{SMB} = z\rho a^{-1} \tag{1}$$

where SMB is in kg m^{-2} a^{-1}, z is depth (m) of the dated layer, ρ (kg m^{-3}) is the density at that depth, and a (years) is the age of the layer. For the Tambora layer in the 2011 IceBridge profiles a is 196 years.

The ice surface firn and near-surface firn are considered to be actively ablating, and SMB rates are negative when the internal layers are truncated at the surface (Figures 3b and 3c). Negative SMB is quantified by the SMB difference of the first truncated internal layer (SMB = 0) and the Tambora layer.

In all three profiles, we observe significant fading of the internal layers in the ablation zones (Figures 3b and S1). This is probably due to intense firn recrystallization and density changes as accumulation drops below about 20 kg m^{-2} a^{-1} and the surface is potentially exposed to intense seasonal thermal cycling for decades to centuries [*Arcone et al.*, 2012; *Courville et al.*, 2007; *Scambos et al.*, 2012]. A secondary potential cause of reduced layer reflections is the presence of some narrow crevassing and firn-cracking [*Severinghaus et al.*, 2010] on the steeper slopes of the wind scoured area. Where the Tambora layer appears to be truncated with significant fading, we linearly interpolate the SMB rates to zero (Figure 3c). However, the actual mass loss may be greater.

3.2. Dating Internal Layers: Methodology, Hypothesis, and Tests

For deriving accumulation rates from snow radar, the internal layers are dated and the continuous layers are assumed to be isochronous [*Eisen et al.*, 2008; *Sinisalo et al.*, 2013]. Ideally, the radar profiles should be connected to an ice core for estimating the age of the internal layers. In this case, the IceBridge radar lines did not intersect any existing ice core site or the 2009 NUS profile. Consequently, we use the layer deposition pattern (dark and light layers in the radiostratigraphy) of the 2009 NUS profile from the surface to a depth of ~20 m to match and date the internal layers of the Profiles 1–3 (Figures 2 and S1). We assume that if the accumulation rates do not vary much between our study area and the location of the NUS firn cores and radar profiles (Figure S3 and Table S1 in the supporting information), then the deposition patterns in a radar echogram should be identical and can be used for dating.

We first test the hypothesis that the near-surface deposition pattern of the 2009 NUS profile and the IceBridge profiles can be linked for dating by comparing SMB rates between the two regions. We use the average depth of the Tambora layer identified in the 2009 NUS profile and in the normal accumulation zone of Profile 1 (0–3 km; Figure 3b). Using equation (1) and appropriate values of ρ, we estimate average SMB rates of 48.4 and 53.7 kg m^{-2} a^{-1} for the 2009 NUS profile and the IceBridge profile, respectively. These rates are very similar to each other and to the RACMO2.3 estimates of 52 kg m^{-2} a^{-1} over our study area (Table S1).

We further test the accuracy of the presumed Tambora layer by using equation (2) to calculate the age of a second internal layer. This method has been previously used to date shallow layers sandwiched between a dated layer and the ice surface assuming uniform effective internal vertical strain rates [*MacGregor et al.*, 2015].

$$a = a_{\mathrm{bot}} \ln(1 - z/H)/\ln(1 - z_{\mathrm{Tam}}/H) \tag{2}$$

where a (years) is the age of the layer, a_{bot} is age of the bottom layer (the Tambora peak), z and z_{Tam} are the mean depths (m) of Layer 2, and the Tambora layer, H, is the ice thickness (average 2400 m here).

We chose a bright reflector (Layer 2; Figures 2 and S4) away from the scour zones at an average 4.5 m depth in Profile 1 and estimate its age at 53 years using equation (1). This age is close to the Agung volcanic peak (1965) identified in NUS ice cores at ~4.9 m near the 2009 NUS reference profile [*Anschütz et al.*, 2011].

Based on these tests, we conclude that we can use the 2009 NUS profile to date the IceBridge profiles and identify the Tambora layer within our study area. The depth of the presumed Tambora layer in normal accumulation regions in our study area ranges from 13 to 18 m (Figure 2). This depth is similar to the average depth of the Tambora layer on the East Antarctic plateau [*Anschütz et al.*, 2011; *Müller et al.*, 2010].

In the redeposition zone, we derive SMB by dating the unconformity using ice surface velocity [*Rignot et al.*, 2011]. We assume that the age of the unconformity at the ice surface where it originates is zero and increases as it moves away from the surface due to ice flow. We also test the consistency of this technique by comparing the SMB rates derived using an unconformity and the Tambora layer identified in consecutive radargrams (U and T in Figure 4d). SMB derived using the unconformity and 350 kg m^{-3} density matched closely with that using the Tambora peak and its appropriate density. The consistency of SMB derived using different layers such as the Tambora and the unconformity with themselves, RACMO2.3, and the 2009 NUS profile indicates that our techniques used for dating the internal layers and the density assumptions are valid for deriving SMB rates over the wind-scour zones within the study area.

4. Results

4.1. Anatomy of a Wind-Scour Zone

Surface morphology, internal layers, and derived SMB of the wind-scour zones are shown in Figures 3 and 4 and S1 and S5. In the normal accumulation zones (Figures 3b and 3c, 4b, 4d, and S1), the radar-derived

Table 1. Distribution of Mass Over the Wind-Scour Zones

Length of the Profiles	Net Mass Loss ($kg\,a^{-1}$)	Snow in Redeposition Zone ($kg\,a^{-1}$)	Length of the Ablation Zones in the Profiles (km)	Net Mass Loss/Length of the Ablation Zone ($kg\,a^{-1}\,km^{-1}$)	Surface Slope Along the Ablation Zone
Profile 1 (28 km)	57.5×10^3	3.21×10^3	12	4.8×10^3	0.006
Profile 2 (36 km)	106×10^3	10.4×10^3	16	6.6×10^3	0.01

accumulation rates match that of RACMO2.3, indicating that (1) we have correctly identified the Tambora layer and (2) RACMO2.3 matches with observations away from wind-scour zones. The profiles show increased MSWD (>0.002) and grain size (>100 μm; Figures 4e and 4f), typical over wind-scour zones [*Das et al.*, 2013; *Scambos et al.*, 2012].

IceBridge laser altimetry-derived surface roughness (Text S5B) and Worldview imagery reveal that the ablation zones can have both smooth/glazed (Figures 3a and S5b), as well as crevassed and scalloped features (Figures 3a and S5c and S5d). Rougher surfaces can influence SMB by increasing sublimation rates due to enhanced turbulent mixing in the near-surface atmosphere, enhanced transport of water vapor through the firn cracks, and also by partially recapturing wind-blown snow (Text S5A).

4.2. Variation of Ablation and Redeposition Rates Over the Wind-Scour Zones

The profiles indicate a complex relationship between ablation rates with surface slopes and length of the scour zones (Table 1). For Profile 1 (surface slope ~0.006, 12 km ablation zone), the lowest observed SMB is $-27\,kg\,m^{-2}\,a^{-1}$ (-27 mm water equivalent (we) a^{-1}), and for Profile 2 (surface slope ~0.01, 16 km ablation zone) it is $-54\,kg\,m^{-2}\,a^{-1}$ (-54 mm we a^{-1}). This ablation process is likely in balance with the ice flow and probably does not change ice sheet elevation. These limited observations indicate that both surface slope and length of the scour zone determine the ablation rate. Wind-scour zones form over steeper ice surface topography and longer wind-scour zones allow the gravity-driven katabatic winds to further increase in speed, resulting in enhanced ablation of the ice surface. Consequently, the ablation rate per kilometer for Profile 2 is almost one and a half times larger than that of Profile 1 probably because Profile 2 has a larger ablation zone (Table 1).

For both profiles, the snow mass accumulated downslope is less than the mass loss over the scour zones. The net ablation over Profile 1 is $58\times10^3\,kg\,a^{-1}$, while the net mass gain at the redeposition zone is only $3\times10^3\,kg\,a^{-1}$, representing ~6% of the total mass loss (Figure 3c). Profile 2 has a total mass loss estimated at $106\times10^3\,kg\,a^{-1}$ with a gain of only $10\times10^3\,kg\,a^{-1}$ in the redeposition zone, representing ~10% of the mass loss (Figures 4b and S2a). Thus, our profiles show that ~90–94% of the ablated mass over the scour zone is sublimated.

Direct measurements of surface sublimation rates are estimated at $54\,kg\,m^{-2}\,a^{-1}$ at 2230 m above sea level (asl) near Mizuho Station, East Antarctica (70.69°S, 44.34°E) for the period 1977–1978 over a wind-scoured/glazed surface [*Fujii and Kusunoki*, 1982]. This rate is similar to the average of the maximum sublimation rates observed in Profiles 1 and 2 estimated at $54\,kg\,m^{-2}\,a^{-1}$ for elevations ranging between 1200 and 1700 m. This study also reported a condensation rate of only 1.1% of the annual sublimation rate. Another study reports a surface sublimation rate of ~$35\,kg\,m^{-2}\,a^{-1}$ near the South Pole [*Stearns and Weidner*, 2013].

Profile 3 has a complex surface topography with multiple wind-scour zones (Figures 4c and S1b). We observe truncation of internal layers and increased grain size at ~25 km (Figures 4d and 4f). This profile also has a larger topographic depression downslope of the wind-scour zone resulting in higher redeposition rate compared to the other profiles. However, we cannot identify the Tambora peak for a significant portion of the ablation zone due to layer fading and hence cannot compare the amount of ablation to redeposition.

4.3. Uncertainties in Radar-Derived Surface Accumulation Rates

We assign an uncertainty window of 2 m where the Tambora layer can be reasonably identified (usually in the accumulation zone) and a 5 m uncertainty window where the layers fade in the ablation zone (Figure S6). The corresponding uncertainties in SMB are estimated at 6% in the accumulation and 17% in the ablation zone (Text S6 and Figure S7). The unconformity can be picked within ±0.25 m. However, the SMB values derived using the unconformity also include errors in ice surface velocities and density assumptions and are difficult to constrain (Figures S6a and S6b).

For quantifying uncertainties due to density assumptions, we use the spread in density at a given depth (Figure S2 and Text S6). Away from the scour zones, the Tambora layer is identified between 13 and 18 m where the density ranges from $563 \pm 43\,kg\,m^{-3}$ and $641 \pm 36\,kg\,m^{-3}$ corresponding to ~6–8% uncertainty in SMB estimates (Text S6 and Figure S8).

5. Discussion

We dated the Tambora and the unconformal layers because the similarity of the background accumulation rates allowed the deposition patterns between our study area located at ~1700–1300 m elevation and NUS cores ~2500 m asl to be matched. Here we compare our radar-derived background rates with other estimates in the region. The NUS08-5 and 6 ice cores nearest to the 2009 NUS profile indicate accumulation rates of 37.6 ± 2.3 and $49.2 \pm 3.4\,kg\,m^{-2}\,a^{-1}$, respectively [*Anschütz et al.*, 2011]. Our reprocessed SMB using the Tambora depth from the 2009 NUS profile and the mean density profile estimated at $\sim 48\,kg\,m^{-2}\,a^{-1}$ agrees with $\sim 53–62\,kg\,m^{-2}\,a^{-1}$ estimated using the IceBridge profiles. These rates also agree with RACMO2.3 estimates of $\sim 40–70\,kg\,m^{-2}\,a^{-1}$ between our study area and the NUS region. On the other hand, *Arthern et al.* [2006] shows a larger SMB gradient ranging from $\sim 35\,kg\,m^{-2}\,a^{-1}$ at the NUS sites to $\sim 100\,kg\,m^{-2}\,a^{-1}$ in our study area. Other studies over the Recovery region and Adélie Land [*Anschütz et al.*, 2011; *Verfaillie et al.*, 2012] also report that *Arthern et al.* [2006] systematically overestimates SMB due to scarce in situ measurements, topographic effects, and coarser resolution satellite data. Some studies compile in situ SMB and derive trends between accumulation rates and elevation or distance from the coast [*Favier et al.*, 2013; *Rotschky et al.*, 2007]. These trends generally indicate higher SMB values than observed in the Recovery region, implying that although the spread in in-situ values are real, the trends may not be appropriate everywhere in East Antarctica.

6. Conclusion

SMB rates over the wind-scour zones in the upper Recovery Glacier catchment in East Antarctica exhibit a great degree of heterogeneity. Our observations reveal a gradual ablation of 16–18 m of firn with SMB rates $\sim -50\,kg\,m^{-2}\,a^{-1}$ (-50 mm we a^{-1}) over ~200 years. This ablation of firn is a persistent process, and the ablation rates are also dependent on the length of the scour zones. The redeposition rates are $<10\%$ of the mass loss indicating sublimation of ice mass. We are aware that these numbers are along the radar profiles and may not accurately represent the total redeposition in the region. Additionally, our study area may have fewer topographic depressions or dunes to recapture wind-blown snow. Nevertheless, our results show that the largest uncertainty in SMB rates from RCMs in East Antarctica is from the wind-scour zones over both ablation and redeposition areas. The sublimation rates at these mid-elevation regions of the ice sheet may be typical of other scour zones and therefore represent a very significant factor in the continental ice mass balance.

Acknowledgments

Funding for this work was provided by NASA grants NNX14AH79G and NNX13AD25A and the Netherlands Polar Program. The IceBridge airborne radar and laser altimetry data used in this work were downloaded through the IceBridge portal "nsidc.org/icebridge/portal/" and also through the CReSIS ftp site: ftp://data.cresis.ku.edu/data/snow/2011_Antarctica_DC8/. The InSAR velocity data were downloaded from NASA DAAC at the National Snow and Ice Data Center doi:10.5067/MEASURES/CRYOSPHERE/nsidc-0484.001. The authors thank P. Morin and Polar Geospatial Center for providing the WorldView imageries used in this work. The authors gratefully acknowledge M. Frezzotti for reviewing the manuscript before submission and A. Sinisalo and H. Anschutz for providing Figure 2a. The authors are also thank M. van Wessem, J. Paden, J. MacGregor, G. Picard, S. Arcone, R. Bell, J. Cochran, E. Isaksson, A. Royer, and M. Wolovick for providing data sets and valuable suggestions.

The Editor thanks Steve Arcone and an anonymous reviewer for their assistance in evaluating this paper.

References

Anschütz, H., A. Sinisalo, E. Isaksson, J. R. McConnell, S. E. Hamran, M. M. Bisiaux, D. Pasteris, T. A. Neumann, and J. G. Winther (2011), Variation of accumulation rates over the last eight centuries on the East Antarctic Plateau derived from volcanic signals in ice cores, *J. Geophys. Res.*, *116*, D20103, doi:10.1029/2011JD015753.

Arcone, S. A., R. Jacobel, and G. Hamilton (2012), Unconformable stratigraphy in East Antarctica: Part I. Large firn cosets, recrystallized growth, and model evidence for intensified accumulation, *J. Glaciol.*, *58*(208), 240–252.

Arthern, R. J., D. P. Winebrenner, and D. G. Vaughan (2006), Antarctic snow accumulation mapped using polarization of 4.3-cm wavelength microwave emission, *J. Geophys. Res.*, *111*, D06107, doi:10.1029/2004JD005667.

Bamber, J. L., J. L. Gomez-Dans, and J. A. Griggs (2009), A new 1 km digital elevation model of the Antarctic derived from combined satellite radar and laser data – Part 1: Data and methods, *Cryosphere*, *3*(1), 101–111.

Barral, H., C. Genthon, A. Trouvilliez, C. Brun, and C. Amory (2014), Blowing snow in coastal Adélie Land, Antarctica: Three atmospheric-moisture issues, *Cryosphere*, *8*(5), 1905–1919.

Bintanja, R. (2000), Snowdrift suspension and atmospheric turbulence. Part I: Theoretical background and model description, *Bound. Layer Meteorol.*, *95*(3), 343–368.

Courville, Z. R., M. R. Albert, M. A. Fahnestock, L. M. Cathles, and C. A. Shuman (2007), Impacts of an accumulation hiatus on the physical properties of firn at a low-accumulation polar site, *J. Geophys. Res.*, *112*, F02030, doi:10.1029/2005JF000429.

Das, I., R. E. Bell, T. A. Scambos, M. Wolovick, T. T. Creyts, M. Studinger, N. Frearson, J. P. Nicolas, J. T. M. Lenaerts, and M. R. van den Broeke (2013), Influence of persistent wind scour on the surface mass balance of Antarctica, *Nat. Geosci.*, *6*(5), 367–371.

Eisen, O., M. Frezzotti, C. Genthon, E. Isaksson, O. Magand, M. R. Van Den Broeke, D. A. Dixon, A. Ekaykin, P. Holmlund, and T. Kameda (2008), Ground-based measurements of spatial and temporal variability of snow accumulation in East Antarctica, *Rev. Geophys.*, *46*, RG2001, doi:10.1029/2006RG000218.

Fahnestock, M. A., T. A. Scambos, C. A. Shuman, and R. J. Arthern (2000), Snow megadune fields on the East Antarctic Plateau: Extreme atmosphere-ice interaction, *Geophys. Res. Lett.*, *27*(22), 3719–3722, doi:10.1029/1999GL011248.

Favier, V., C. Agosta, S. Parouty, G. Durand, G. Delaygue, H. Gallée, A. S. Drouet, A. Trouvilliez, and G. Krinner (2013), An updated and quality controlled surface mass balance dataset for Antarctica, *Cryosphere*, *7*(2), 583–597.

Frezzotti, M. R., S. Gandolfi, F. La Marca, and S. Urbini (2002), Snow dunes and glazed surfaces in Antarctica: New field and remote-sensing data, *Ann. Glaciol.*, *34*(1), 81–88.

Frezzotti, M. R., C. Scarchilli, S. Becagli, M. Proposito, and S. Urbini (2013), A synthesis of the Antarctic surface mass balance during the last 800 yr, *Cryosphere*.

Frezzotti, M., S. Urbini, M. Proposito, C. Scarchilli, and S. Gandolfi (2007), Spatial and temporal variability of surface mass balance near Talos Dome, East Antarctica, *J. Geophys. Res.*, *112*, F02032, doi:10.1029/2006JF000638.

Fujii, Y., and K. Kusunoki (1982), The role of sublimation and condensation in the formation of ice sheet surface at Mizuho Station, Antarctica, *J. Geophys. Res.*, *87*(C6), 4293–4300, doi:10.1029/JC087iC06p04293.

Goodwin, I. D. (1990), Snow accumulation and surface topography in the katabatic zone of eastern Wilkes Land, Antarctica, *Antarct. Sci.*, *2*(3), 235–242.

Lenaerts, J. T. M., M. R. van den Broeke, W. J. van de Berg, E. van Meijgaard, and P. K. Munneke (2012a), A new, high-resolution surface mass balance map of Antarctica (1979–2010) based on regional atmospheric climate modeling, *Geophys. Res. Lett.*, *39*, L04501, doi:10.1029/2011GL050713.

Lenaerts, J. T. M., M. R. van den Broeke, S. J. Dery, E. van Meijgaard, W. J. van de Berg, S. P. Palm, and J. S. Rodrigo (2012b), Modeling drifting snow in Antarctica with a regional climate model: 1. Methods and model evaluation, *J. Geophys. Res.*, *117*, D05108, doi:10.1029/2011JD016145.

MacGregor, J. A., M. A. Fahnestock, G. A. Catania, J. D. Paden, S. Prasad Gogineni, S. K. Young, S. C. Rybarski, A. N. Mabrey, B. M. Wagman, and M. Morlighem (2015), Radiostratigraphy and age structure of the Greenland Ice Sheet, *J. Geophys. Res. Earth Surf.*, *120*, 212–241, doi:10.1002/2014JF003215.

Medley, B., et al. (2014), Constraining the recent mass balance of Pine Island and Thwaites glaciers, West Antarctica, with airborne observations of snow accumulation, *Cryosphere*, *8*(4), 1375–1392.

Müller, K., A. Sinisalo, H. Anschütz, S.-E. Hamran, J.-O. Hagen, J. R. McConnell, and D. R. Pasteris (2010), An 860 km surface mass-balance profile on the East Antarctic plateau derived by GPR, *Ann. Glaciol.*, *51*(55), 1–8.

Palm, S. P., Y. K. Yang, J. D. Spinhirne, and A. Marshak (2011), Satellite remote sensing of blowing snow properties over Antarctica, *J. Geophys. Res.*, *116*, D16123, doi:10.1029/2011JD015828.

Rignot, E., J. Mouginot, and B. Scheuchl (2011), Ice flow of the Antarctic ice sheet, *Science*, *333*(6048), 1427–1430.

Rotschky, G., P. Holmlund, E. Isaksson, R. Mulvaney, H. Oerter, M. R. Van Den Broeke, and J.-G. Winther (2007), A new surface accumulation map for western Dronning Maud Land, Antarctica, from interpolation of point measurements, *J. Glaciol.*, *53*(182), 385–398.

Scambos, T. A., et al. (2012), Extent of low-accumulation 'wind glaze' areas on the East Antarctic plateau: Implications for continental ice mass balance, *J. Glaciol.*, *58*(210), 633–647.

Scarchilli, C., M. Frezzotti, P. Grigioni, L. De Silvestri, L. Agnoletto, and S. Dolci (2010), Extraordinary blowing snow transport events in East Antarctica, *Clim. Dynam.*, *34*(7–8), 1195–1206.

Severinghaus, J. P., et al. (2010), Deep air convection in the firn at a zero-accumulation site, central Antarctica, *Earth Planet. Sci. Lett.*, *293*(3–4), 359–367.

Shepherd, A., et al. (2012), A reconciled estimate of ice-sheet mass balance, *Science*, *338*(6111), 1183–1189.

Sinisalo, A., H. Anschütz, A. T. Aasen, K. Langley, A. Deschwanden, J. Kohler, K. Matsuoka, S. E. Hamran, M. J. Øyan, and E. Schlosser (2013), Surface mass balance on Fimbul ice shelf, East Antarctica: Comparison of field measurements and large-scale studies, *J. Geophys. Res. Atmos.*, *118*, 11,625–11,635.

Stearns, C. R., and G. A. Weidner (2013), Sensible and latent heat flux estimates in Antarctica, in *Antarctic Meteorology and Climatology: Studies Based on Automatic Weather Stations*, pp. 109–138, AGU, Washington, D. C.

van den Broeke, M. R. (1997), Spatial and temporal variation of sublimation on Antarctica: Results of a high-resolution general circulation model, *J. Geophys. Res.*, *102*(D25), 29,765–29,777, doi:10.1029/97JD01862.

van den Broeke, M. R., J. G. Winther, E. Isaksson, and J. F. Pinglot (1999), Climate variables along a traverse line in Dronning Maud Land, East Antarctica, *J. Glaciol.*, *45*(150), 295–302.

Van Wessem, J. M., et al. (2014), Improved representation of East Antarctic surface mass balance in a regional atmospheric climate model, *J. Glaciol.*, *60*(222), 761–770.

Verfaillie, D., M. Fily, E. Le Meur, O. Magand, B. Jourdain, L. Arnaud, and V. Favier (2012), Snow accumulation variability derived from radar and firn core data along a 600 km transect in Adelie Land, East Antarctic plateau, *Cryosphere*, *6*(6), 1345–1358.